npj computational materials

www.nature.com/npjcompumats

ARTICLE OPEN

Check for updates

Installing a molecular truss beam stabilizes MOF structures

Hong Ki Kim[1,2,4], Jong-Yeong Jung[1,4], Gyumin Kang[1,2], Mu-Hyun Baik[1,2]✉ and Eun-Young Choi[1,3]✉

Enhancing the stability and durability of metal-organic frameworks (MOFs) is vital for practical applications because many promising MOF materials suffer from phase transitions and/or structural decompositions with humidity being a particularly damaging condition. In mechanical engineering, the frame of buildings and furniture can be stabilized significantly by installing a truss beam. Employing the same principle, we functionalized the organic component of MOF-5 to contain a carbazole moiety that can act as a molecular truss beam by reaching across the corner and forming a stable π–π interaction with a phenyl group on the edge position of the MOF-skeleton. This structural support enhanced the stability of the MOF substantially, allowing the designed MOF to maintain compositional integrity under steam conditions at 90 °C for ~5 days. The unmodified MOF-5 shows clear signs of structural collapse after ~1 h.

npj Computational Materials (2022)8:117 ; https://doi.org/10.1038/s41524-022-00799-3

INTRODUCTION

The compositional tunability of metal-organic frameworks (MOFs) that take advantage of the inherent porosity and large surface areas by interconnecting inorganic metal nodes and multitopic organic ligands has provided a diverse opportunity for tailoring their physicochemical properties. By combining different metal ions and organic ligands, various framework matrices can be formed that display a variety of pore sizes, channel types, shapes, and functionalities[1–3]. The versatility of these materials can be further enhanced by functionalization of the components before assembly or post-synthetic modification (PSM)[4] techniques that enable the fabrication of porous materials with high compositional and structural complexities. MOFs have found a number of promising applications such as chemical separation[5–7], gas storage[8–11], heterogeneous catalysis[12–14], molecule sensing[15,16], or ion conduction[17,18]. A serious weakness of many MOFs that often limits their utility in practical and industrial applications is that they undergo phase transformations and decompositions. Water is particularly damaging for many MOF materials[19–22]. For example, the iconic materials MOF-5[23] and HKUST-1[24], consisting of $Zn_4O(bdc)_3$ and $Cu_3(btc)_2$ (H_2bdc = 1,4-benzenedicarboxylic acid; H_3btc = 1,3,5-benzenetricarboxylic acid), were extensively examined for the aforementioned applications but were found to be too unstable. The exposure of MOF-5 to humid air under ambient conditions gives rise to a transformation of the high-surface-area MOF-5 to low-surface-area MOF-69c or MOF-5W[25,26]. Several strategies were tested for enhancing the hydrolytic stability of MOFs:[27] (i) the organic ligands were modified to be more hydrophobic[28–31], (ii) tri- or tetra-valent metal cations such as Fe^{3+}, Al^{3+}, Cr^{3+}, and Zr^{4+} were employed to strengthen the metal–ligand bonds[32–36], (iii) nitrogen-containing ligands were engaged with low-valent metal ions[37,38], (iv) interpenetration systems were designed to stabilize MOF structures[39], and (v) ligands were rigidified to strengthen the stability of the framework[40].

Based on a combined computational and experimental exploration, we found that the stability of MOFs can be increased significantly using a simple mechanical approach to strengthening the MOF skeleton. Truss beams have been used in building and furniture construction since ancient Egyptian ages to stabilize rectangular constructs. We hypothesized that a molecular truss beam that can reach across the corner angles of the MOF cage may increase the structural integrity in a similar fashion, as conceptualized in Fig. 1. To the best of our knowledge, this simple and general approach has not been explored for enhancing the stability and durability of MOFs. To test the validity of this approach, we constructed a MOF that shares the same structural skeleton with MOF-5, but one ligand carries a functional group such as a carbazole that can reach across the corner angle to the other ligand in the cage and function as a molecular truss beam. Specifically, 2,5-bis(*n*-(9H-carbazol-9-yl)-propoxy)-1,4-benzenedicarboxylic acid (CZ*n*-H_2bdc) and 1,4-benzenedicarboxylic acid (H_2bdc) ligands were used in combination with Zn^{2+} ions to build the structurally stabilized MOFs.

RESULTS AND DISCUSSION

Design and Modeling of Structurally Stable MOFs

We chose a typical isoreticular cubic nanocrystal MOF-5 that consists of multiple frames with zinc oxide tetrahedral units, (Zn_4O), connected by 1,4-benzenedicarboxylic acid (H_2bdc) ligands forming an alternating chain where each phenyl group is twisted by 90° and their lattice has a $[Zn_4O(bdc)_3]_8$ stoichiometry in a unit cell[23]. MOF-5 is known to have no coordinatively unsaturated metal sites, unlike HKUST-1 that adopts a Cu–Cu paddle-wheel structure and features open coordination sites that can bind small molecules such as H_2O, EtOH, MeOH, and MeCN[41]. Nevertheless, the hydrolytic stability of MOF-5 is much lower than that of HKUST-1 due to the pliable structure of the weak $Zn–O_{bdc}$ bonds that allow for water molecules to attack the Zn sites, followed by phase transformation or structural collapse[26,42]. Therefore, both blocking the water from accessing the metal sites and strengthening the structural rigidity of MOFs may enhance the hydrolytic stability of MOF materials. Previously, various functionalized H_2bdc derivatives with nonpolar aliphatic groups were used to improve the hydrolytic stability by installing

[1]Department of Chemistry, Korea Advanced Institute of Science and Technology (KAIST), Daejeon 34141, Republic of Korea. [2]Center for Catalytic Hydrocarbon Functionalizations, Institute for Basic Science (IBS), Daejeon 34141, Republic of Korea. [3]Korea Science Academy of KAIST, 105-47 Baegyanggwanmun-ro, Busanjin-gu, Busan 47162, Republic of Korea. [4]These authors contributed equally: Hong Ki Kim, Jong-Yeong Jung. ✉email: mbaik2805@kaist.ac.kr; faujasite1@kaist.ac.kr

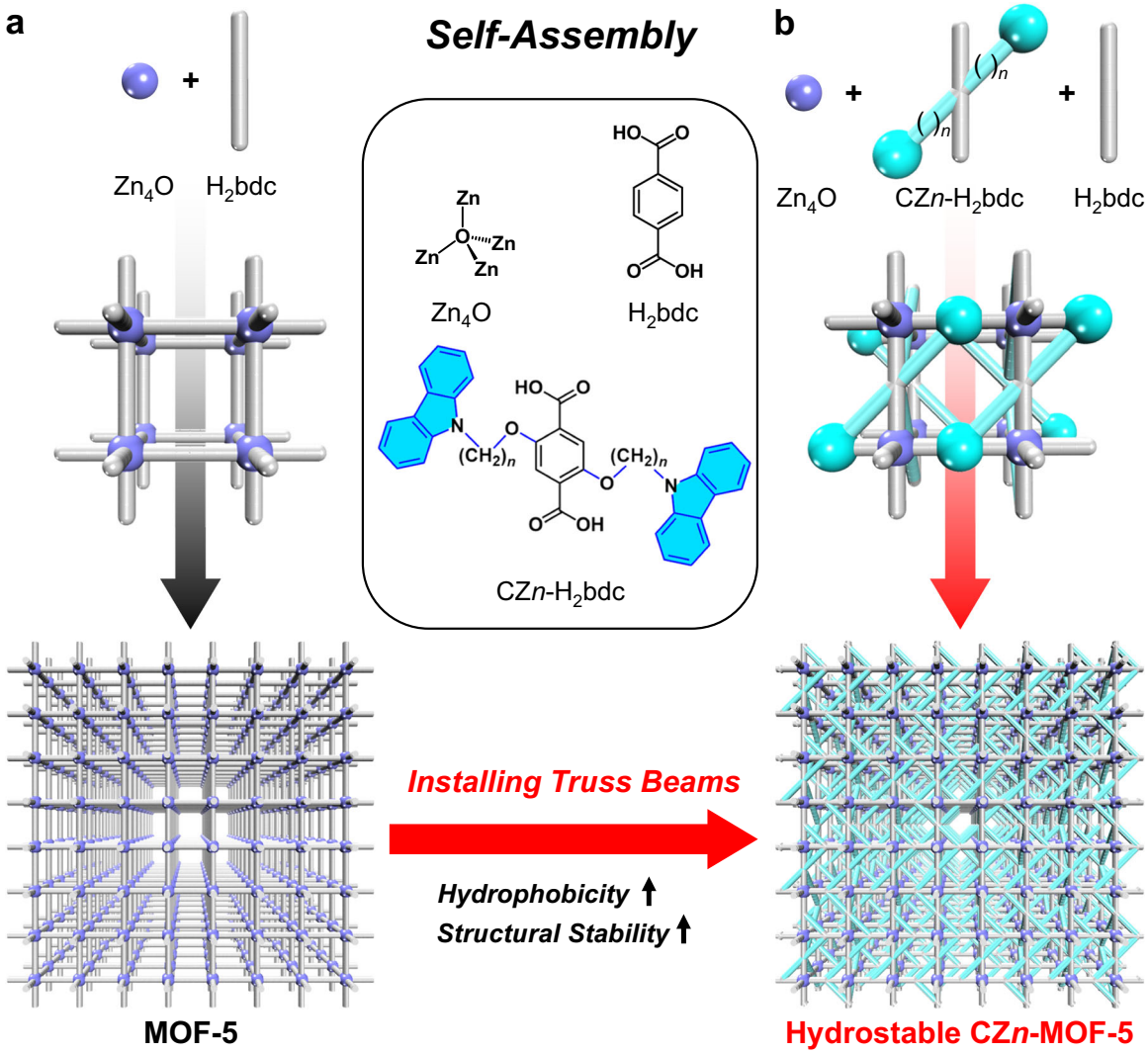

Fig. 1 Schematic illustration of installing a molecular truss beam to enhance hydrolytic stability of metal-organic frameworks. a MOF-5. **b** CZ*n*-MOF-5 by shielding the zinc oxide site and rigidifying the frameworks in a combination of 1,4-benzenedicarboxylic acid (H_2bdc) and 2,5-bis(*n*-(9H-carbazol-9-yl)-propoxy)-1,4-benzenedicarboxylic acid (CZ*n*-H_2bdc) ligands ($n = 3$ and 10).

hydrophobic surfaces within the MOFs[28,43–45]. In particular, the incorporation of short functional groups is attractive because the branches have little impact on the porosity and gas adsorption capability of the MOF materials. Aliphatic groups were found to be less effective[43,44].

To enhance both the structural stability and hydrophobicity of MOFs, we took inspiration from building and furniture construction where rectangular angles are structurally stabilized by truss beams, as shown in Fig. 1. After some iterative computational and experimental explorations, we concluded that a promising strategy for installing a molecular truss beam is to combine two different ligands, where only one carries functional groups that are designed to reach across the rectangular angle of the MOF cage to strongly interact with the other ligand.

Exploratory studies revealed that carbazole functionalities that can be easily installed on the MOF-skeleton are well-suited for our strategy, and Fig. 2 illustrates the shapes of the frontier orbitals of H_2bdc and CZ3-H_2bdc ligands. The lowest unoccupied molecular orbital (LUMO) of H_2bdc and CZ3-H_2bdc is simply a π^*-orbital, and the highest occupied molecular orbital (HOMO) of the CZ3-H_2bdc ligand is a π-orbital derived from the pendent carbazole group. Thus, the pendent carbazole group of the CZ3-H_2bdc ligand can act as a π-donor, whereas the central phenyl groups of the H_2bdc and the CZ3-H_2bdc are π-acceptors. Therefore, the CZ3-H_2bdc ligands can act as a molecular truss beam by reaching across the corner and forming a stable face-to-face π–π interaction.

Quantum chemical calculations indicated that the CZ*n*-H_2bdc ligand is particularly effective when used in combination with the unfunctionalized H_2bdc ligand. As highlighted in Fig. 3, the arene functionalities of the carbazole moiety in CZ*n*-H_2bdc can engage the arene group of the neighboring H_2bdc ligand to form strong π–π interactions, which effectively serves as the truss beam that we imagined. The length of the alkyl tether with which the carbazole is attached to the H_2bdc ligand can be varied easily, and our calculations showed that a three methylene tether is ideal (i.e. CZ3-H_2bdc). In addition to providing structural support that structurally stabilizes the MOF skeleton, these truss beam constructs afford hydrophobic conditions and block the channel that could be used by water molecules to approach the metal site.

To test the proposed construct, computer models were constructed employing periodic boundary conditions using CZ3-H_2bdc ligands based on the MOF-5 unit cell structure ($(Zn_4O)_8(bdc)_{24}$) by considering intermolecular interactions such as steric hindrance, van der Waals forces, hydrogen bonding, and

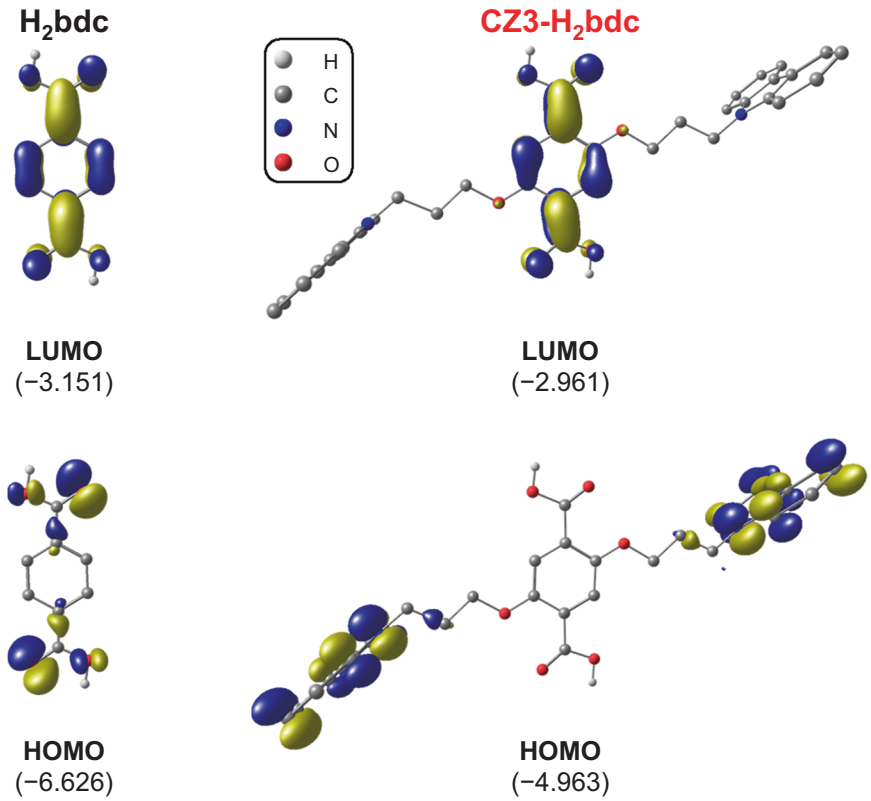

Fig. 2 Isosurface plots (isodensity value = 0.05 a.u.) of HOMO and LUMO of the H_2bdc and CZ3-H_2bdc ligands. Electronic energies (eV) are in parenthesis. Non-essential hydrogens are not shown.

noncovalent interactions according to Eq. 1:

$$(Zn_4O)_8(bdc)_{24} + x\text{CZ3-bdc}^{2-} \rightarrow (Zn_4O)_8(bdc)_{24-x}(\text{CZ3-bdc})_x + x\text{bdc}^{2-} \quad (1)$$

As shown in Fig. 3, the structures of $[(Zn_4O)_8(bdc)_{24}]$, MOF-5, and the designed $[(Zn_4O)_8(bdc)_{16}(\text{CZ3-bdc})_8]$ were geometrically optimized with density functional theory based tight-binding (DFTB) methods that are suitable for treating very large systems. Interestingly, we found that two major interactions support the truss beam forming interactions: (i) a strong π–π interaction between the arene functionalities of the carbazole and the H_2bdc moieties, (ii) a non-classical hydrogen bonding interaction between the carboxylate oxygen of the ligand and the alkyl-hydrogen of the tethering group of the carbazole in the CZ*n*-H_2bdc ligand. The non-classical hydrogen bond has sufficient influence over the molecular structures[46,47], and its bond strength is estimated to be in the range of 2–3 kcal mol^{-1}. The hydrogen bonding (C–H···O_{bdc}) with a bond length of ~2 Å gives assistance to the orientation of carbazole groups toward the tetrahedral zinc oxide cluster that is an obvious water-vulnerable site. More significantly, a substantial anchoring effect is exerted by a π–π interaction at a phenyl-phenyl distance of 3.685 Å, tightly tethering the carbazole group that can reach across to the other ligand (See Fig. 3b). These noncovalent interactions (NCIs) were further confirmed (Fig. 3c and Supplementary Fig. 1)[48]. Thus, these calculations suggested that structural stability is significantly enhanced, which should allow for conserving the compositional integrity of the MOF under humid conditions.

Synthesis and Characterization

Under solvothermal reaction conditions, self-assembly reactions between $Zn(NO_3)_2{\cdot}6H_2O$ and H_2bdc in *N,N*-diethylformamide (DEF) afforded transparent microcrystals of MOF-5. The CZ3-MOF-5 materials were prepared following the identical protocol by combining the Zn sources with a mixture of CZ3-H_2bdc and H_2bdc ligands (See Fig. 4). Although the crystals differ notably in color, they showed the same cubic crystal morphology owing to the identical connectivity and similarity of the dicarboxylate-based building blocks, as shown in Fig. 4a, b.

To confirm the computationally predicted installment of the molecular truss beam, we sought to identify the π–π interaction in CZ*n*-MOF-5 using diffuse reflectance ultraviolet-visible (UV-vis) spectroscopy (Fig. 4 and Supplementary Fig. 2). The UV–vis absorption of the MOF-5 is dominated by the signature of the phenyl group of the H_2bdc ligands. On the other hand, the CZ3-H_2bdc ligands showed a dyad spectrum based on a combination of the central phenyl group and the pendent carbazole group[49]. Notably, the absorption peaks were observed at 290 nm and 326 nm, as shown in Fig. 4d, which are assigned to the aforementioned π-donor-acceptor interaction in the CZ3-MOF-5. To further confirm this key interaction, solid-state Cross-Polarization Magic Angle Spinning Carbon-13 Nuclear Magnetic Resonance (CP/MAS ^{13}C NMR) analysis was employed. The solid-state NMR spectra at a spinning rate of 12 kHz showed the de-shielding and shielding effect of carbons affected by π–π interaction (See Supplementary Fig. 3). Also, we investigated the FT-IR spectra paying special attention to the symmetric and asymmetric carboxylate stretching modes of CZ3-H_2bdc ligand at $\tilde{\nu}$ = 1610 cm^{-1} and 1600 cm^{-1}, respectively, in the two different MOFs while the free ligand shows C=O stretching at $\tilde{\nu}$ = 1736 cm^{-1} (Fig. 4e). The C–N stretching mode at $\tilde{\nu}$ = 1320 cm^{-1} due to the carbazole group is clearly visible in the CZ3-MOF-5 spectrum. Finally, ^{1}H NMR studies were conducted (See Fig. 4f and Supplementary Fig. 4). The CZ3-MOF-5 sample dissolved in a mixture of DCl/D_2O and DMSO-d_6 solution displayed four identical protons in H_2bdc at 8.02–8.04 ppm and two identical protons in CZ3-H_2bdc are found at 7.24–7.28 ppm, confirming that the CZ3-

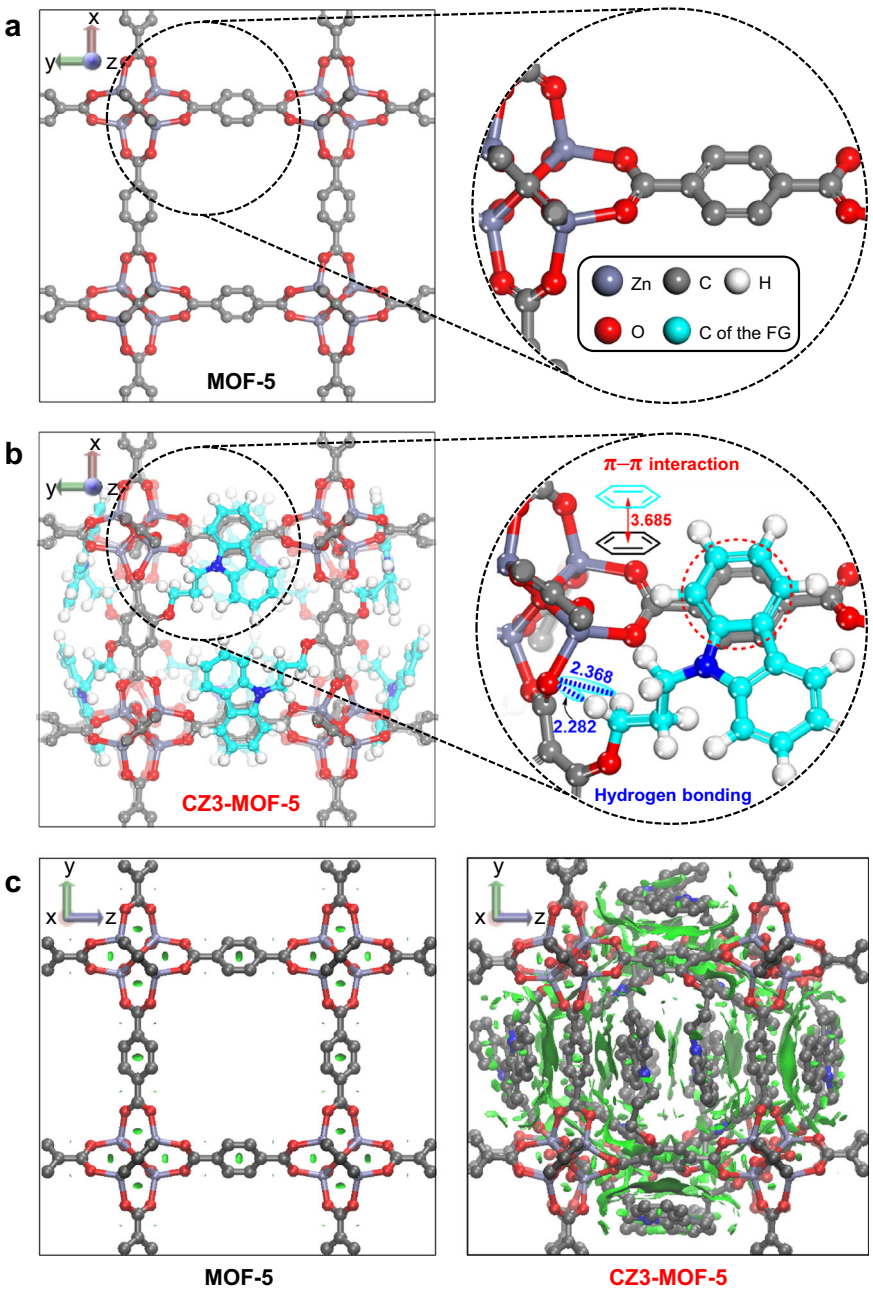

Fig. 3 Computed structures in a unit cell. a MOF-5. **b** CZ3-MOF-5. **c** Non-covalent interaction (NCI) plots of the MOF-5 and the CZ3-MOF-5. All bond lengths are in Å. The surface of the NCI interactions is colored on a green scale. Non-essential hydrogens are not shown.

MOF-5 material was successfully prepared. Comparing the peak integration of the ^{1}H NMR signals of the H_2bdc to that of CZ3-H_2bdc, a ratio of ~2.3:1 is found, which is consistent with the compositional ratio suggested by our calculations for the designed $[(Zn_4O)_8(bdc)_{16}(CZ3\text{-}bdc)_8]$ system. Moreover, for the CZ10-MOF-5 sample, the ratio of H_2bdc to CZ10-H_2bdc is analyzed to ~3.7:1 due to spatial constraints imposed by the bulkiness of pendent groups of the CZ10-H_2bdc ligand (See Supplementary Fig. 4).

Hydrolytic stability test

The MOF-5 and CZ3-MOF-5 samples were exposed to moisture under steam conditions at 90 °C and were examined using powder X-ray diffraction (PXRD) to test their structural integrity, as shown in Fig. 5, Supplementary Fig. 5, and Supplementary Fig. 6. The main peaks near 6.8° and 9.7° of the CZ3-MOF-5 are nearly identical to that of MOF-5, and the overall diffraction patterns are similar to the CZ3-MOF-5 sample giving more intense signals, as illustrated in Fig. 5c and Fig. 5d, suggesting that the isoreticular structural frameworks are similar. These diffraction patterns are in good agreement with our computationally optimized structures that showed practically identical framework configurations, as illustrated in Fig. 5a, b, Supplementary Fig. 7, and Supplementary Fig. 8. The PXRD patterns show that exposure to moisture leads to a structural collapse of MOF-5 within an hour, and a phase transition to MOF-5W takes place, indicated by a diffraction peak that appears at $2\theta = 8.8°$[26]. In contrast, the CZ3-MOF-5 micro-crystals maintained the PXRD patterns even after 5 days and showed a very small peak that indicated a minor phase transition after 6 days, displaying remarkable stability (Fig. 5d). These

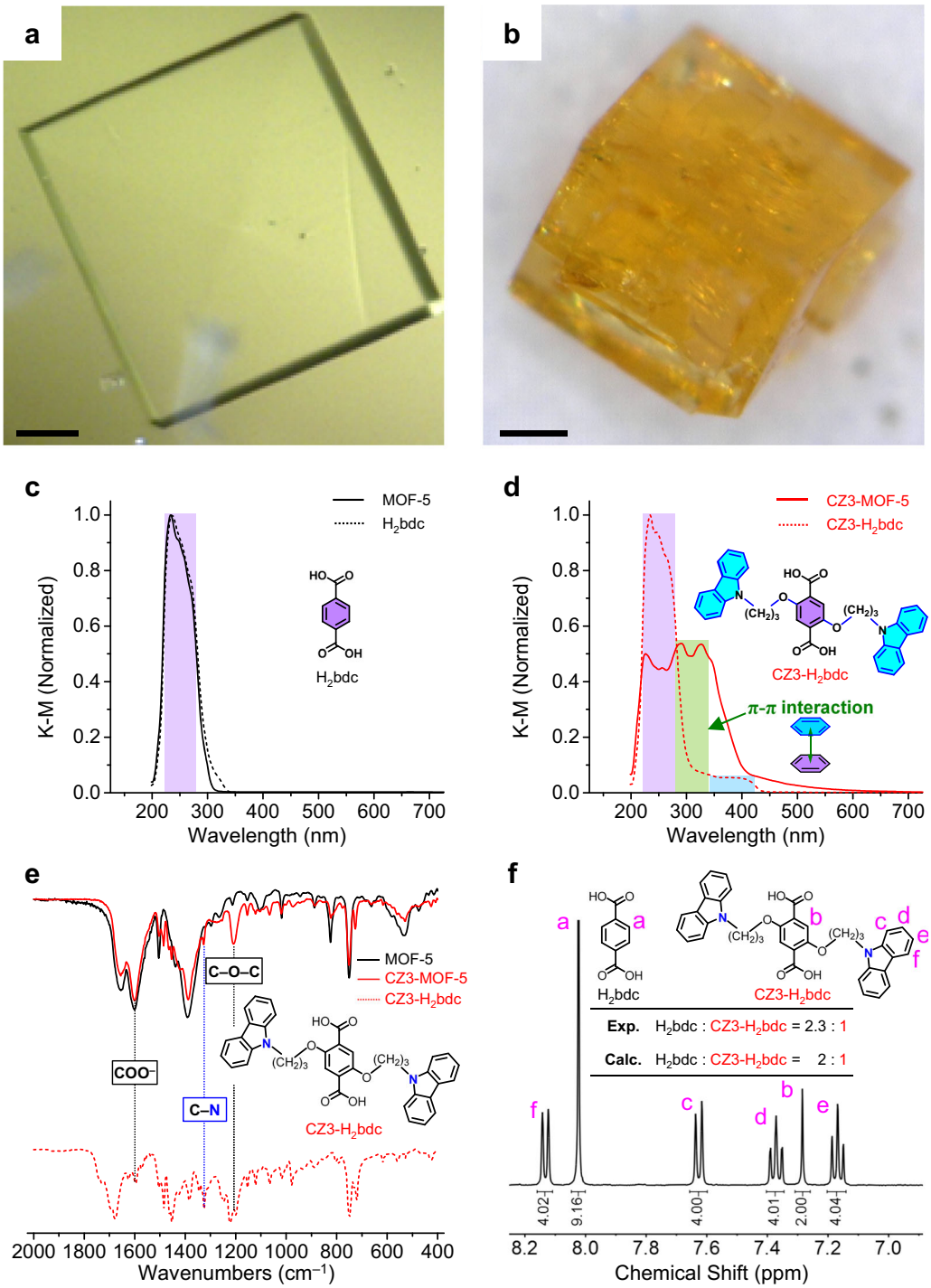

Fig. 4 Experimental characterizations of samples. Optical microscope images of **a** MOF-5 and **b** CZ3-MOF-5. Diffuse reflectance UV–vis absorption spectra of **c** H_2bdc, MOF-5, and **d** CZ3-H_2bdc, CZ3-MOF-5. **e** FT-IR spectra of MOF-5, CZ3-H_2bdc, and CZ3-MOF-5. **f** ^{1}H NMR spectrum of CZ3-MOF-5 dissolved in a mixture of DCl/D_2O and DMSO-d_6 solution. Inset: A peak integration ratio of the ^{1}H NMR signals for the ligands. Scale bars, 0.1 mm (**a**) and 0.1 mm (**b**).

observations confirm that molecular truss beams are effective for structurally stabilizing the MOF-skeleton.

Molecular dynamics simulations

We carried out DFTB molecular dynamics (MD) simulations to better understand the molecular basis for the observed differences in hydrolytic stabilities of MOF-5 and CZ3-MOF-5 microcrystals, including water molecules at 298 K and 1 atm in a periodic simulation box (Fig. 6 and Supplementary Fig. 9). It is challenging to capture chemical events such as bond breaking and structural collapse with standard MD simulations, because these events take place in time scales of several seconds, if not hours, while computer simulations can only probe a much shorter time scale. Nonetheless, a careful analysis of the MD simulations can provide much insight into how water molecules approach the vulnerable sites. Previous studies reported that water molecules interact with the MOF-5 by directly attacking the Zn_4O moiety via

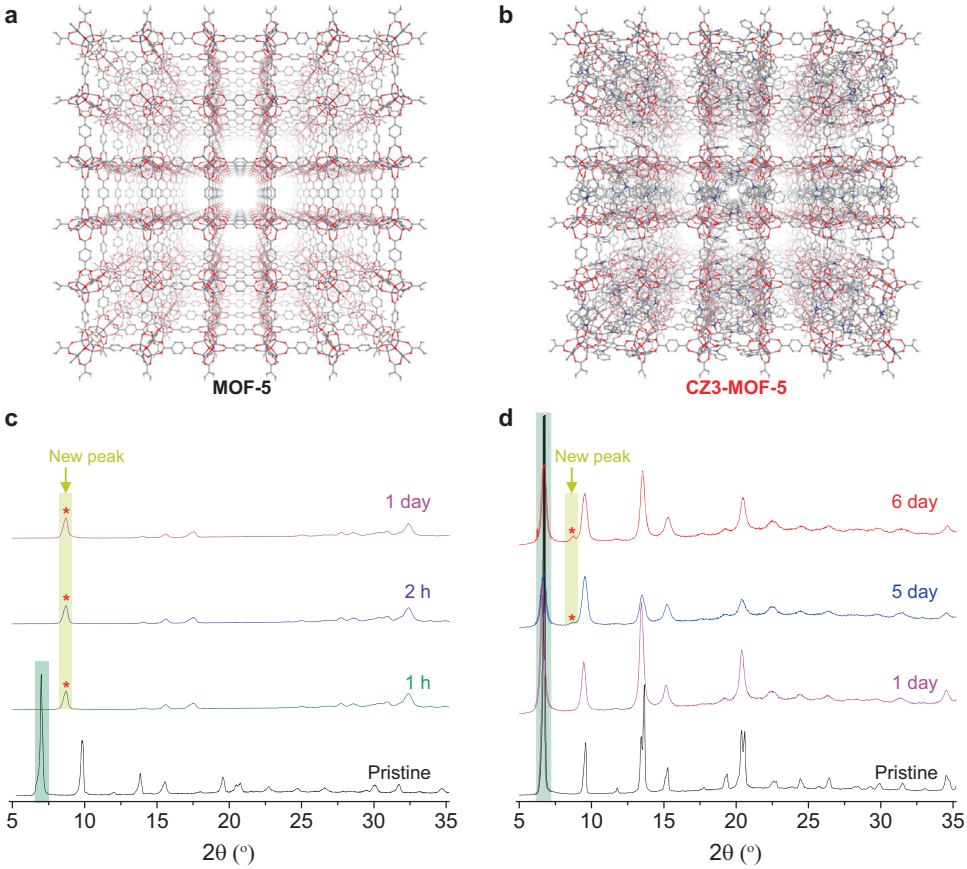

Fig. 5 Hydrolytic stability with respect to the exposure time to steam at 90 °C. Perspective views of **a** MOF-5 and **b** CZ3-MOF-5 in the supercell (3 × 3 × 3). PXRD patterns of **c** MOF-5 and **d** CZ3-MOF-5. The asterisk and yellow marks highlight the appearance of a peak at about 8.8° due to the phase transformation of MOF-5 to MOF-5W.

a ligand exchange mechanism where water replaces one of the coordination bonds of MOF-5 ($Zn–O_{bdc}$)[22,50]. Hydrogen bonding interaction between H_2O and O_{bdc} sites was also identified as important for the structural degradation.

In our MD simulations, we prepare the initial state by filling the void in the MOF with randomly oriented water molecules that match a liquid density of ~0.998 g mL^{-1}, which is then equilibrated for standard conditions. These calculations reveal that the vulnerable metal-ligand contact sites in MOF-5 attract clusters of hydrogen-bonded water molecules, as shown in Fig. 6a. All hydrogen bonding interactions shorter than 2.3 Å that qualify as strong are highlighted in sky blue dash lines[51]. During the MD simulations, we observed an attack of water molecules on the tetrahedral Zn_4O unit to strongly coordinate to the Zn atom with $Zn–OH_2$ bond length being 2.15 Å. Among the hydrogen-bonded network of water molecules, a representative hydrogen bonding interactions ($O_{bdc}\cdots H_2O$) that will serve a starting point for attacking the carboxylate moiety of the organic ligand is highlighted in yellow in Fig. 5a. As a result of the interactions between MOF-5 and the water molecules, the $Zn–O_{bdc}$ bonds are notably elongated to ~2.46 Å, and the frameworks are highly distorted (Fig. 6a). In contrast, the $Zn–O_{bdc}$ bonds on the CZ3-MOF-5 are maintained at a relatively short 1.94 and 2.03 Å after 100 ps. The simulation shows that the alkyl-tethered carbazole not only provides structural integrity by maintaining the anchoring effect on the MOF-skeleton but plays a crucial role in repelling water attacks, and discourages the formation of hydrogen-bonded water clusters at the vulnerable sites. These results highlight that the structural support combined with the classical approach of increasing the hydrophobicity is in play synergistically to afford the hydrostability.

N_2 isotherms and specific surface areas

The N_2 isotherm characteristics of CZ3-MOF-5 was explored next. As mentioned above, decorating the organic ligands with large or bulky functional groups can affect the porosity and the internal surface area and other physicochemical properties. Before experimentally testing a gas adsorption/desorption isotherms, we first examined the electrostatic potential (ESP) map of H_2bdc, CZ3-H_2bdc, MOF-5 and CZ3-MOF-5 cluster models from each unit cell structure (Table 1 and Supplementary Fig. 10). Previously, more polarizable adsorbents with electrostatic potentials that show higher amplitudes exhibited increased abilities to adsorb gases[52]. As shown in Table 1, the MOF-5 and CZ3-MOF-5 clusters show similar electrostatic potentials as isostructural frameworks except for the pendent carbazole moiety of the CZ3-H_2bdc ligand, which displays a notably higher degree of charge polarization. These calculations indicate that CZ3-MOF-5 features a much more polarizable framework surface than MOF-5, which may induce a more robust interaction with adsorbent molecules.

Previously, a systematic investigation of the N_2 adsorption sites in MOF-5 was performed using both experimental and computational methods[53,54]. The N_2 molecules primarily adsorb on the Zn_4O tetrahedral sites in the MOF-5 at low loadings. As suggested by the aforementioned studies, the Zn_4O sites of the CZ3-MOF-5 are moderately obscured by the pendent carbazole groups, which reduces the favorable binding sites in CZ3-MOF-5 compared to MOF-5. Consequently, the accessible surface area is expected to be smaller in the trust beam stabilized MOF. Our studies show that

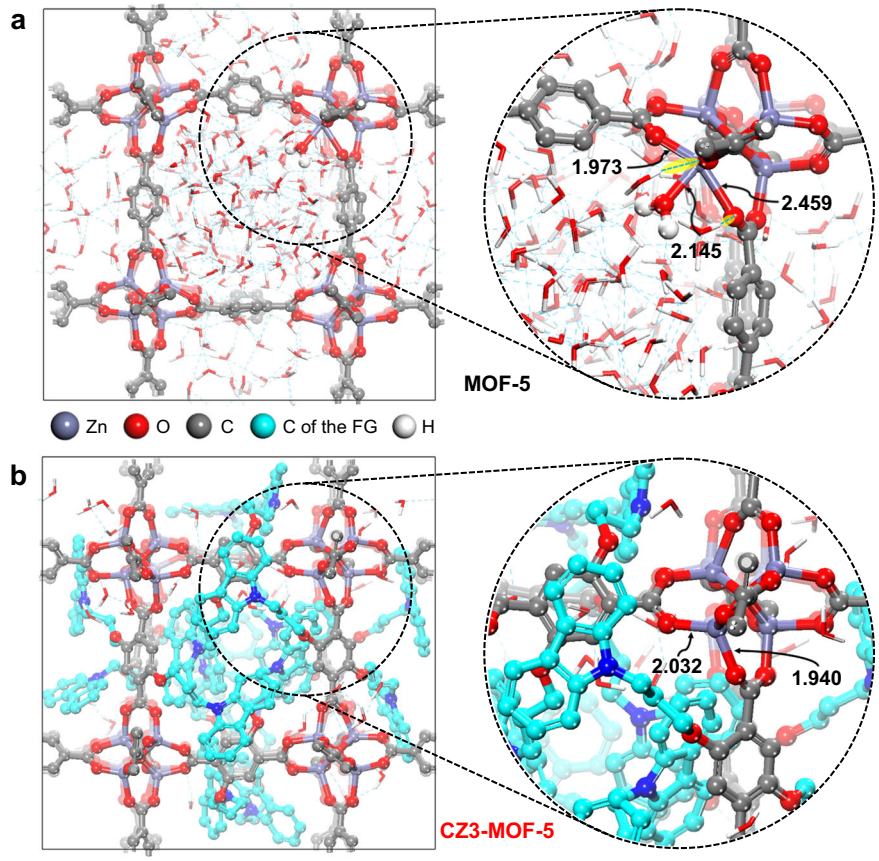

Fig. 6 Snapshots for the equilibrium state based on the DFTB molecular dynamics simulation after 100 ps. a MOF-5. **b** CZ3-MOF-5. The number of H_2O molecules was determined with current density ~0.998 g mL^{-1} in the periodic boundary condition. Non-essential hydrogens are not shown.

Table 1. Electrostatic potential (ESP) maps and specific surface areas of MOF-5 and CZ3-MOF-5.

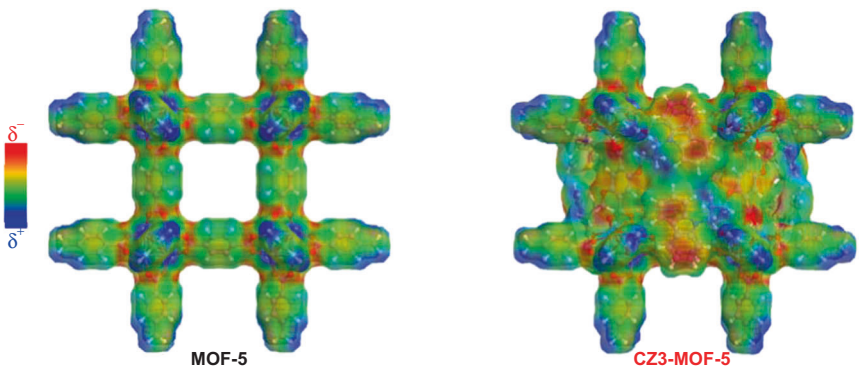

MOF	Ligand	S_{BET}[a] (m^2 g^{-1})	S_{Lang}[b] (m^2 g^{-1})
MOF-5	H_2bdc	3170.6	3417.6
CZ3-MOF-5	H_2bdc + CZ3-H_2bdc	1344.3	1445.1

[a]S_{BET} = BET surface area. [b]S_{Lang} = Langmuir surface area.

the BET and Langmuir surface areas of the CZ3-MOF-5 are 1344 $m^2\ g^{-1}$ and 1445 $m^2\ g^{-1}$ (Table 1, Supplementary Fig. 11, and Supplementary Table 1), respectively, which is indeed smaller than 3171 $m^2\ g^{-1}$ and 3418 $m^2\ g^{-1}$, seen for MOF-5, respectively. Thus, the carbazole functionality provided robust MOF structures with great hydrolytic stability and moderate surface areas as a truss beam component. To more improve the surface area, a structurally simpler construct that does not interfere with the binding site of the guest molecules may be preferable.

We developed a rational design strategy for increasing the stability of MOF matrices by installing a molecular truss beam that reaches across a rectangular corner of the MOF-skeleton, employing the same principles that structurally stabilize buildings and furniture. A prototype MOF designed to serve as a proof of principle of this strategy, CZ*n*-MOF-5, showed remarkably high structural integrity evidenced by enhanced water-resistance under steam conditions at 90 °C for 5 days. A detailed computational and experimental analysis suggests that the increased stability is the result of a synergistic interplay between increased strength of the lattice and increased hydrophobicity in the MOF cavity. Whereas the carbazole functionality was convenient for this demonstration, as it can readily engage in a strong π–π stacking interaction across the corner, it obscures the nitrogen binding site and notably reduces the active binding surface compared to the parent MOF construct. Our simple strategy inspired by how truss beams are used in everyday life should be generally applicable for stabilizing all MOF-type structures and offers an orthogonal, potentially synergistic approach to conventional strategies. Of particular interest are molecular truss beams that are structurally simpler and are anchored more tightly, for example using covalent bonds across the corner. Efforts towards preparing such MOFs are underway in our laboratories.

METHOD

Computational details

All calculations were performed with the density functional-based tight-binding (DFTB) theory[55,56] as implemented in the Amsterdam Modeling Suite (AMS) products of SCM. Geometry optimizations and molecular dynamics (MD) simulations were performed using the GFN-xTB model[57]. The simulated system was a cubic cell with three-dimensional periodic boundary conditions. In the MD simulations, the time step was chosen to be 1 fs, which is relatively short but adequate for the purposes of this study. The simulation time for equilibrium states was 100 ps in 100,000 steps. The number of H_2O molecules was determined for a liquid density of ~0.998 g mL^{-1} in the periodic boundary condition. Non-covalent interaction (NCI) was calculated based on the level of promolecular approximation implemented in NCIPLOT 3.0[48,58] and the surface of NCIs was visualized by Visual Molecular Dynamics (VMD)[59] software. The electrostatic potential (ESP) calculations for H_2bdc, CZ3-H_2bdc, MOF-5, and CZ3-MOF-5 cluster models were performed by single-point calculations with the PBE-D3/6-31G** level of theory[60–62] with zinc represented by the Los Alamos LACVP basis set[63–65] in Jaguar 9.1[66]. The ESP maps were obtained using the Jmol[67] software. The HOMO and LUMO energies of the H_2bdc and the CZ3-H_2bdc were reevaluated by single-point calculations using Dunning's correlation consistent triple-ζ basis set cc-pVTZ(-f) that includes a double set of polarization functions[68].

DATA AVAILABILITY

The datasets generated during the current study are available from the corresponding author on reasonable request.

CODE AVAILABILITY

Jaguar (schrodinger.com/jaguar), DFTB (scm.com/product/dftb), JMOL (jmol.org), Chemcraft (chemcraftprog.com), and VMD (ks.uiuc.edu/Research/vmd) are available from their websites.

Received: 16 December 2020; Accepted: 28 April 2022;
Published online: 24 May 2022

REFERENCES

1. Yaghi, O. M., Li, H., Davis, C., Richardson, D. & Groy, T. L. Synthetic strategies, structure patterns, and emerging properties in the chemistry of modular porous solids. *Acc. Chem. Res.* **31**, 474–484 (1998).
2. Zhou, H.-C., Long, J. R. & Yaghi, O. M. Introduction to metal-organic frameworks. *Chem. Rev.* **112**, 673–674 (2012).
3. Zhou, H.-C. & Kitagawa, S. Metal-organic frameworks (MOFs). *Chem. Soc. Rev.* **43**, 5415–5418 (2014).
4. Deria, P. et al. Beyond post-synthesis modification: evolution of metal-organic frameworks via building block replacement. *Chem. Soc. Rev.* **43**, 5896–5912 (2014).
5. Bae, Y.-S. et al. High propene/propane selectivity in isostructural metal-organic frameworks with high densities of open metal sites. *Angew. Chem. Int. Ed.* **51**, 1857–1860 (2012).
6. Luo, F. et al. UTSA-74: a MOF-74 isomer with two accessible binding sites per metal center for highly selective gas separation. *J. Am. Chem. Soc.* **138**, 5678–5684 (2016).
7. Cadiau, A., Adil, K., Bhatt, P. M., Belmabkhout, Y. & Eddaoudi, M. A metal-organic framework-based splitter for separating propylene from propane. *Science* **353**, 137–140 (2016).
8. Krause, S. et al. A pressure-amplifying framework material with negative gas adsorption transitions. *Nature* **532**, 348–352 (2016).
9. Eddaoudi, M. et al. Systematic design of pore size and functionality in isoreticular MOFs and their application in methane storage. *Science* **295**, 469–472 (2002).
10. Dincă, M. & Long, J. R. Hydrogen storage in microporous metal-organic frameworks with exposed metal sites. *Angew. Chem. Int. Ed.* **47**, 6766–6779 (2008).
11. Bae, Y.-S. & Snurr, R. Q. Development and evaluation of porous materials for carbon dioxide separation and capture. *Angew. Chem. Int. Ed.* **50**, 11586–11596 (2011).
12. Lee, J. et al. Metal-organic framework materials as catalysts. *Chem. Soc. Rev.* **38**, 1450–1459 (2009).
13. Trickett, C. A. et al. Identification of the strong Brønsted acid site in a metal-organic framework solid acid catalyst. *Nat. Chem.* **11**, 170–176 (2019).
14. Zhang, X. et al. Catalytic chemoselective functionalization of methane in a metal −organic framework. *Nat. Catal.* **1**, 356–362 (2018).
15. Kreno, L. E. et al. Metal-organic framework materials as chemical sensors. *Chem. Rev.* **112**, 1105–1125 (2012).
16. Gassensmith, J. J. et al. A metal-organic framework-based material for electrochemical sensing of carbon dioxide. *J. Am. Chem. Soc.* **136**, 8277–8282 (2014).
17. Ramaswamy, P., Wong, N. E. & Shimizu, G. K. H. MOFs as proton conductors - challenges and opportunities. *Chem. Soc. Rev.* **43**, 5913–5932 (2014).
18. Sheberla, D. et al. Conductive MOF electrodes for stable supercapacitors with high areal capacitance. *Nat. Mater.* **16**, 220–224 (2017).
19. Kaye, S. S., Dailly, A., Yaghi, O. M. & Long, J. R. Impact of preparation and handling on the hydrogen storage properties of Zn_4O(1,4-benzenedicarboxylate)$_3$ (MOF-5). *J. Am. Chem. Soc.* **129**, 14176–14177 (2007).
20. De Toni, M., Jonchiere, R., Pullumbi, P., Coudert, F.-X. & Fuchs, A. H. How can a hydrophobic MOF be water-unstable? Insight into the hydration mechanism of IRMOFs. *Chemphyschem* **13**, 3497–3503 (2012).
21. Burtch, N. C., Jasuja, H. & Walton, K. S. Water stability and adsorption in metal-organic frameworks. *Chem. Rev.* **114**, 10575–10612 (2014).
22. Han, S. S., Choi, S.-H. & van Duin, A. C. T. Molecular dynamics simulations of stability of metal-organic frameworks against H_2O using the ReaxFF reactive force field. *Chem. Commun.* **46**, 5713–5715 (2010).
23. Li, H., Eddaoudi, M., O'Keeffe, M. & Yaghi, O. M. Design and synthesis of an exceptionally stable and highly porous metal-organic framework. *Nature* **402**, 276–279 (1999).
24. Chui, S. S., Lo, S. M., Charmant, J. P., Orpen, A. G. & Williams, I. D. A chemically functionalizable nanoporous material. *Science* **283**, 1148–1150 (1999).
25. Hausdorf, S., Wagler, J., Mossig, R. & Mertens, F. O. R. L. Proton and water activity-controlled structure formation in zinc carboxylate-based metal organic frameworks. *J. Phys. Chem. A* **112**, 7567–7576 (2008).
26. Rodríguez, N. A., Parra, R. & Grela, M. A. Structural characterization, optical properties and photocatalytic activity of MOF-5 and its hydrolysis products: implications on their excitation mechanism. *RSC Adv.* **5**, 73112–73118 (2015).
27. Duan, J., Jin, W. & Kitagawa, S. Water-resistant porous coordination polymers for gas separation. *Coord. Chem. Rev.* **332**, 48–74 (2017).
28. Jasuja, H., Burtch, N. C., Huang, Y.-G., Cai, Y. & Walton, K. S. Kinetic water stability of an isostructural family of zinc-based pillared metal-organic frameworks. *Langmuir* **29**, 633–642 (2013).

29. Nguyen, J. G. & Cohen, S. M. Moisture-resistant and superhydrophobic metal-organic frameworks obtained via postsynthetic modification. *J. Am. Chem. Soc.* **132**, 4560–4561 (2010).
30. Ma, D., Li, Y. & Li, Z. Tuning the moisture stability of metal-organic frameworks by incorporating hydrophobic functional groups at different positions of ligands. *Chem. Commun.* **47**, 7377–7379 (2011).
31. Cheng, F. et al. Fine-tuning optimal porous coordination polymers using functional alkyl groups for CH_4 purification. *J. Mater. Chem. A* **5**, 17874–17880 (2017).
32. Cavka, J. H. et al. A new zirconium inorganic building brick forming metal organic frameworks with exceptional stability. *J. Am. Chem. Soc.* **130**, 13850–13851 (2008).
33. Férey, G. et al. A chromium terephthalate-based solid with unusually large pore volumes and surface area. *Science* **309**, 2040–2042 (2005).
34. Yang, S. et al. Selectivity and direct visualization of carbon dioxide and sulfur dioxide in a decorated porous host. *Nat. Chem.* **4**, 887–894 (2012).
35. Feng, D. et al. Kinetically tuned dimensional augmentation as a versatile synthetic route towards robust metal-organic frameworks. *Nat. Commun.* **5**, 5723 (2014).
36. Wang, B. et al. Highly stable Zr(IV)-based metal-organic frameworks for the detection and removal of antibiotics and organic explosives in water. *J. Am. Chem. Soc.* **138**, 6204–6216 (2016).
37. Lv, X.-L. et al. A base-resistant metalloporphyrin metal-organic framework for C–H bond halogenation. *J. Am. Chem. Soc.* **139**, 211–217 (2017).
38. He, T. et al. Kinetically controlled reticular assembly of a chemically stable mesoporous Ni(II)-pyrazolate metal-organic framework. *J. Am. Chem. Soc.* **142**, 13491–13499 (2020).
39. Chen, B. et al. A microporous metal-organic framework for gas-chromatographic separation of alkanes. *Angew. Chem. Int. Ed.* **45**, 1390–1393 (2006).
40. Lv, X.-L. et al. Ligand rigidification for enhancing the stability of metal-organic frameworks. *J. Am. Chem. Soc.* **141**, 10283–10293 (2019).
41. Kim, H. K. et al. A chemical route to activation of open metal sites in the copper-based metal-organic framework materials HKUST-1 and Cu-MOF-2. *J. Am. Chem. Soc.* **137**, 10009–10015 (2015).
42. Low, J. J. et al. Virtual high throughput screening confirmed experimentally: porous coordination polymer hydration. *J. Am. Chem. Soc.* **131**, 15834–15842 (2009).
43. Jung, J.-Y. et al. Microporous metal organic framework-based copolymers with efficient gas adsorption capability and high temporal stability. *Macromol. Res.* **25**, 1100–1104 (2017).
44. Yang, J., Grzech, A., Mulder, F. M. & Dingemans, T. J. Methyl modified MOF-5: a water stable hydrogen storage material. *Chem. Commun.* **47**, 5244–5246 (2011).
45. Zhang, Z. et al. Polymer-metal-organic frameworks (polyMOFs) as water tolerant materials for selective carbon dioxide separations. *J. Am. Chem. Soc.* **138**, 920–925 (2016).
46. Jones, C. R., Baruah, P. K., Thompson, A. L., Scheiner, S. & Smith, M. D. Can a C–H···O interaction be a determinant of conformation? *J. Am. Chem. Soc.* **134**, 12064–12071 (2012).
47. Driver, R. W., Claridge, T. D. W., Scheiner, S. & Smith, M. D. Torsional and electronic factors control the C−H···O interaction. *Chem. Eur. J.* **22**, 16513–16521 (2016).
48. Johnson, E. R. et al. Revealing noncovalent interactions. *J. Am. Chem. Soc.* **132**, 6498–6506 (2010).
49. Zhang, J. et al. Self-assembly of electron donor-acceptor-based carbazole derivatives: Novel fluorescent organic nanoprobes for both one- and two-photon cellular imaging. *ACS Appl. Mater. Interfaces* **8**, 11355–11365 (2016).
50. Greathouse, J. A. & Allendorf, M. D. The interaction of water with MOF-5 simulated by molecular dynamics. *J. Am. Chem. Soc.* **128**, 10678–10679 (2006).
51. Jeffrey, G. A. *An Introduction to Hydrogen Bonding*. (Oxford University Press, 1997).
52. Farrusseng, D. et al. Heats of adsorption for seven gases in three metal-organic frameworks: systematic comparison of experiment and simulation. *Langmuir* **25**, 7383–7388 (2009).
53. Rowsell, J. L. C., Spencer, E. C., Eckert, J., Howard, J. A. K. & Yaghi, O. M. Gas adsorption sites in a large-pore metal-organic framework. *Science* **309**, 1350–1354 (2005).
54. Walton, K. S. & Snurr, R. Q. Applicability of the BET method for determining surface areas of microporous metal-organic frameworks. *J. Am. Chem. Soc.* **129**, 8552–8556 (2007).
55. Elstner, M. et al. Self-consistent-charge density-functional tight-binding method for simulations of complex materials properties. *Phys. Rev. B* **58**, 7260–7268 (1998).
56. Gaus, M., Cui, Q. & Elstner, M. DFTB3: Extension of the self-consistent-charge density-functional tight-binding method (SCC-DFTB). *J. Chem. Theory Comput* **7**, 931–948 (2011).
57. Grimme, S., Bannwarth, C. & Shushkov, P. A robust and accurate tight-binding quantum chemical method for structures, vibrational frequencies, and non-covalent interactions of large molecular systems parametrized for all spd-block elements (Z = 1–86). *J. Chem. Theory Comput.* **13**, 1989–2009 (2017).
58. Contreras-García, J. et al. NCIPLOT: a program for plotting non-covalent interaction regions. *J. Chem. Theory Comput.* **7**, 625–632 (2011).
59. Humphrey, W., Dalke, A. & Schulten, K. VMD - visual molecular dynamics. *J. Mol. Graph.* **14**, 33–38 (1996). 27–8.
60. Perdew, J. P., Burke, K. & Ernzerhof, M. Generalized gradient approximation made simple. *Phys. Rev. Lett.* **77**, 3865–3868 (1996).
61. Hehre, W. J., Ditchfield, R. & Pople, J. A. Self—consistent molecular orbital methods. XII. further extensions of Gaussian—type basis sets for use in molecular orbital studies of organic molecules. *J. Chem. Phys.* **56**, 2257–2261 (1972).
62. Grimme, S., Antony, J., Ehrlich, S. & Krieg, H. A consistent and accurate ab initio parametrization of density functional dispersion correction (DFT-D) for the 94 elements H-Pu. *J. Chem. Phys.* **132**, 154104 (2010).
63. Hay, P. J. & Wadt, W. R. Ab initio effective core potentials for molecular calculations. Potentials for the transition metal atoms Sc to Hg. *J. Chem. Phys.* **82**, 270–283 (1985).
64. Wadt, W. R. & Hay, P. J. Ab initio effective core potentials for molecular calculations. Potentials for main group elements Na to Bi. *J. Chem. Phys.* **82**, 284–298 (1985).
65. Hay, P. J. & Wadt, W. R. Ab initio effective core potentials for molecular calculations. Potentials for K to Au including the outermost core orbitals. *J. Chem. Phys.* **82**, 299–310 (1985).
66. Bochevarov, A. D. et al. Jaguar: A high-performance quantum chemistry software program with strengths in life and materials sciences. *Int. J. Quantum Chem.* **113**, 2110–2142 (2013).
67. Hanson, R. M., Willlighaven, E., Vervelle, N., Driscoll, T. & Howard, M. Jmol: an open-source Java viewer for chemical structures in 3D. http://www.jmol.org/ (2008).
68. Dunning Jr., T. H. Gaussian basis sets for use in correlated molecular calculations. I. The atoms boron through neon and hydrogen. *J. Chem. Phys.* **90**, 1007–1023 (1989).

ACKNOWLEDGEMENTS

This work was supported by the Korea Science Academy of KAIST with funds from the Ministry of Science and ICT and the Institute for Basic Science (IBS-R010-A1) in Korea.

AUTHOR CONTRIBUTIONS

H.K.K., J.-Y.J., M.-H.B., and E.-Y.C. conceived the idea and designed the experiments. H.K.K. carried out the computational studies. H.K.K., J.-Y.J., and G.K. synthesized the materials and carried out the experimental analyses. H.K.K. and J.-Y.J., M.-H.B., and E.-Y.C. wrote the manuscript. All authors discussed the results and commented on the manuscript.

COMPETING INTERESTS

The authors declare no competing interests.

ADDITIONAL INFORMATION

Supplementary information The online version contains supplementary material available at https://doi.org/10.1038/s41524-022-00799-3.

Correspondence and requests for materials should be addressed to Mu-Hyun Baik or Eun-Young Choi.

Reprints and permission information is available at http://www.nature.com/reprints

Publisher's note Springer Nature remains neutral with regard to jurisdictional claims in published maps and institutional affiliations.